Contract No:

This document was prepared in conjunction with work accomplished under Contract No. 89303321CEM000080 with the U.S. Department of Energy (DOE) Office of Environmental Management (EM).

Disclaimer:

Savannah River National Laboratory

We put science to work.™

CdZnTeSe: An Emerging Material Toward Advancement of Radiation Detector and Substrate Applications

Utpal N. Roy[1], Giuseppe S. Camarda[2], Yonggang Cui[2], and Ralph B. James[1]

[1]Savannah River National Laboratory, Aiken, SC 29808, USA.

[2]Brookhaven National Laboratory, Upton, NY 11973, USA.

II-VI Workshop 2021

Introduction

CdTe based materials (mainly CdZnTe) are known to be room-temperature semiconductor material for gamma-ray detection as well as substrate material for IR/night vision applications.

CZT suffers from 3 major detrimental defects

- Non-unity segregation of Zn.
- High concentrations of sub-grain boundary and their network.
- High concentrations of Te inclusions/precipitates.

- These issues cause low yield and high cost of CZT radiation detectors and substrate applications.
- Researchers have been trying to solve the issues by improving the crystal growth and post-growth annealing processes but have not mitigated all the disadvantages.

Non-unity segregation coefficient of Zn (~1.35) in CdTe matrix

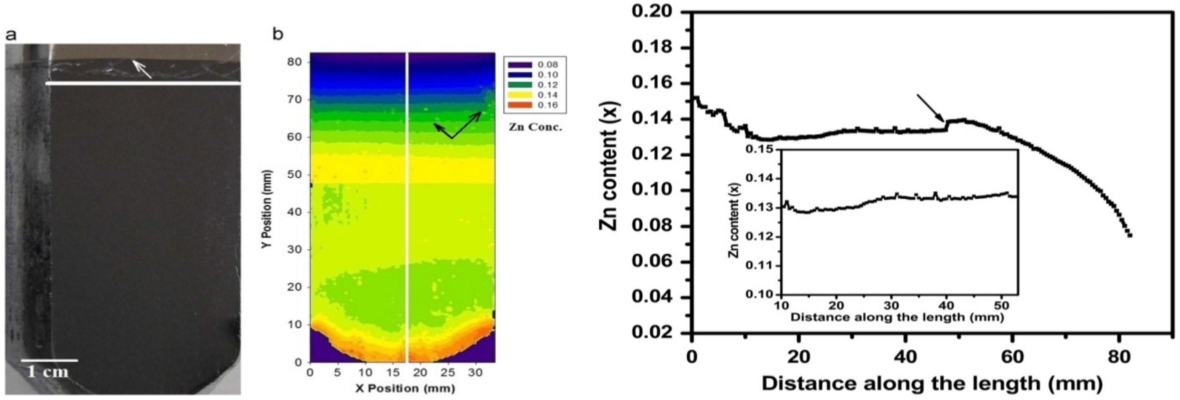

(a) *(b)* *(c)*

(a) THM-grown CZT ingot cut along the length, (b) Zn concentration mapping and (c) Zn concentration along the length of the ingot. *Roy et al. J. Crystal Growth 347 (2012) 53.*

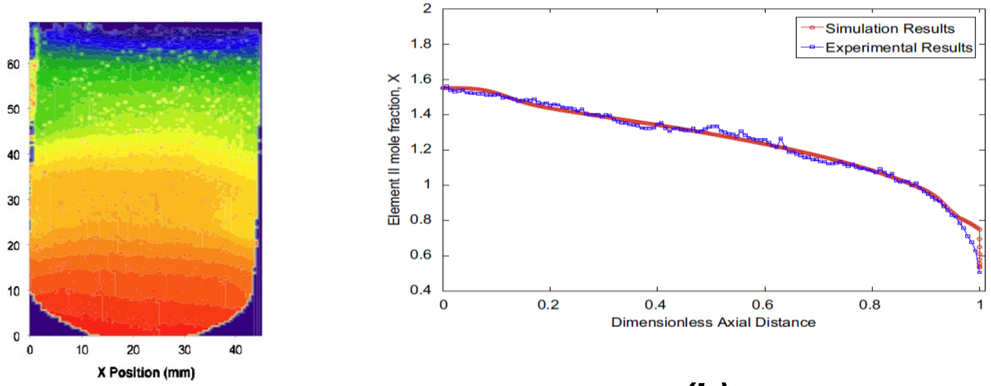

(a) *(b)*

(a) Zn concentration mapping and b) Zn variation along the length of Bridgman-grown ingot. *J. Derby et al. J. Crystal Growth 325 (2011)10.*

Overall yield is highly compromised.

Result: Increased cost of detectors and substrates.

Presence of large concentration of sub-grain boundaries and their network.

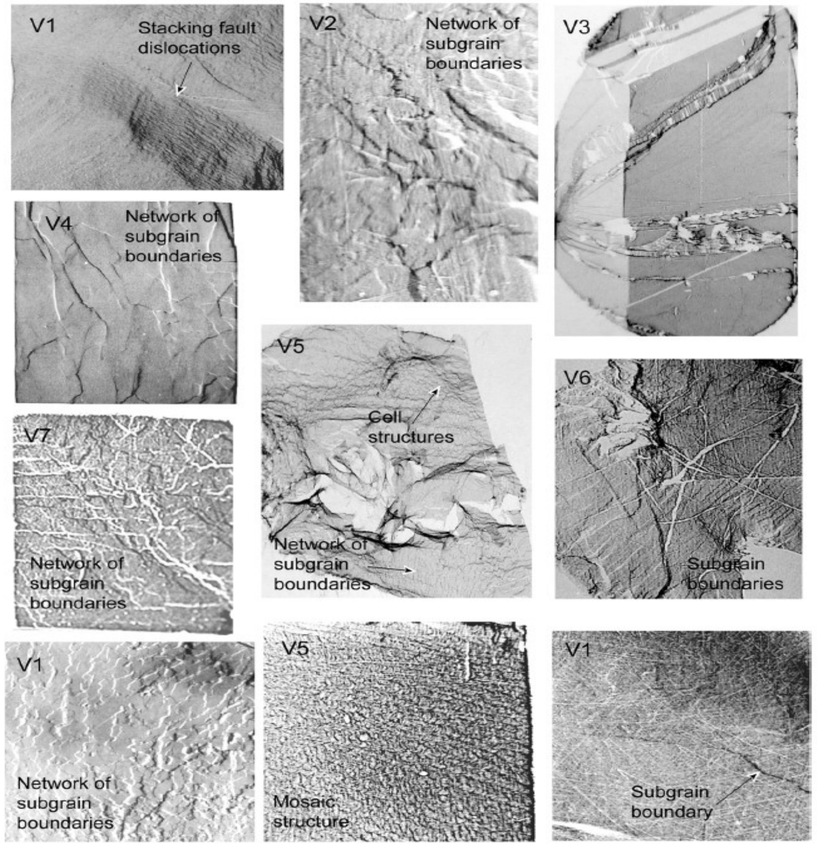

X-Ray diffraction topography images showing ~1 cm^2 areas of detector-grade CZT samples supplied by seven different vendors. A. E. Bolotnikov et al. J. Cryst. Growth 379 (2013) 46.

Effect of sub-grain boundary and their network on CZT device response

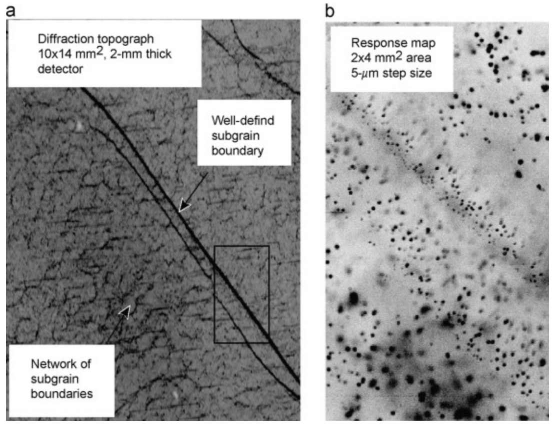

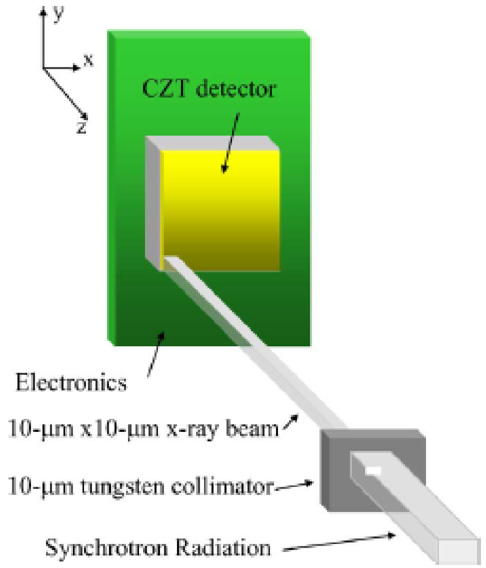

Set-up for the micro-scale mapping of a CZT detector.

X-ray topography and the high-resolution X-ray response map.

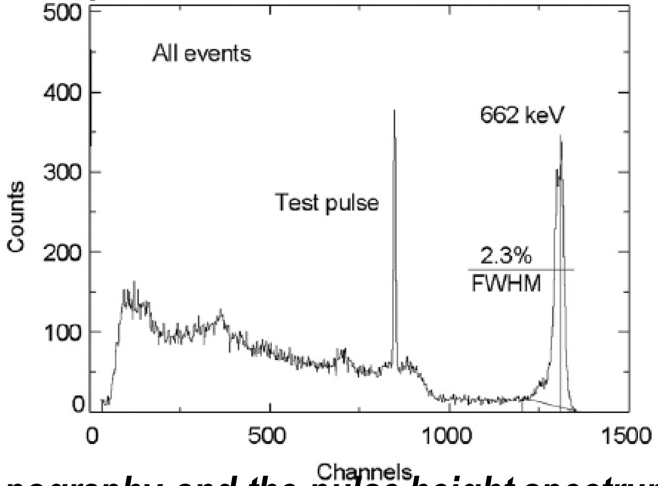

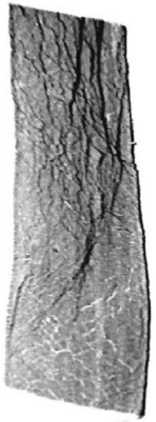

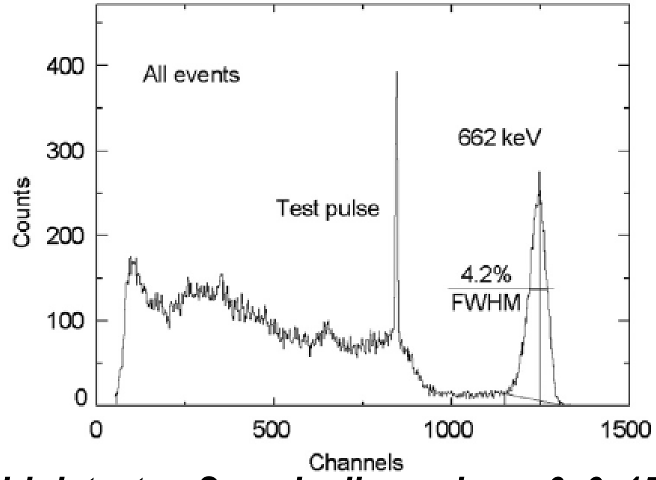

X-ray topography and the pulse height spectrum of CZT Frisch-grid detector. Sample dimensions: 6x6x15 mm^3.

A. E. Bolotnikov et al. J. Cryst. Growth 379 (2013) 46.

Sub-grain boundary networks are responsible for lowering the yield of high-quality detectors.

Te-inclusions/precipitates and their effects on device response

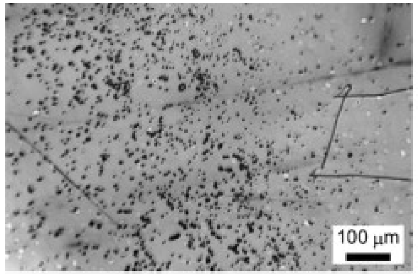

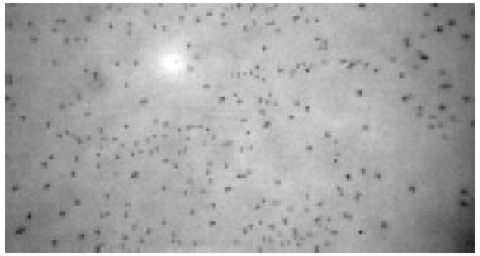

Typical Te inclusions in CdZnTe as observed through IR transmission microscopy.
R. Sekine et al. Cryst. Growth & Design 19 (2019) 6218., S. Szeles, Phys. Stat. Sol. 241 (2004) 783.

Te inclusions however can be eliminated through thermal annealing process, which produces very large diameter (400-500 μm) defects called punching defects. These defects are invisible to IR transmission and severely impede charge transport.

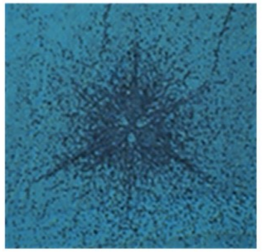

Optical image

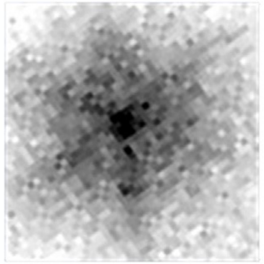

X-ray response map

Details of a 'star-like' defect revealed by optical microscopy imaging of the CZT crystal surface after chemical etching (left) and a map of the electron charge-collection efficiency after synchrotron X-ray response mapping (right).

G. E. Yang et al., JCG 379 (2013) 16.

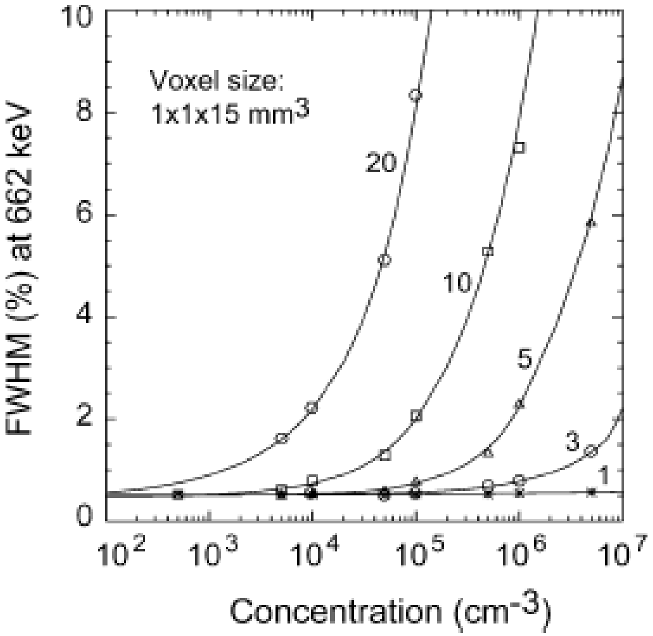

FWHM (%) at 662 keV of the cumulative effect of Te inclusions on energy resolution (after bi-parametric correction) versus their concentration calculated for 1-, 3-, 5-, 10-, and 20- μm inclusions. The detector's length is 15 mm.
A. E. Bolotnikov et al. IEEE Trans. on Nucl. Science 54, 821 (2007).

The key to achieve high-quality detector grade CZT is to minimize Te inclusions.

Effects of defects on the device/substrate quality

- **Non-unity segregation of Zn.**

Results in compositional inhomogeneity along the grown ingot, reduced yield of the useful material.

- **High concentrations of sub-grain boundary and their network.**

For detector applications: Degrades the detector performance heavily.

For substrate applications: Sub-grain boundaries are basically dislocation walls and are prone to propagate to the epitaxial layer during growth.

- **High concentrations of Te inclusions/precipitates.**

For detector applications: Te inclusions are performance limiting defects and affect the detector performance.

For substrate applications: Te inclusions can appear on the surface of the substrate and disrupt the lattice constant, and they are responsible for introducing localized defects in the growing epitaxial layer.

Thus, to increase the overall yield with high quality detectors and substrates, the compositional homogeneity with highly reduced Te inclusions and sub-grain boundary networks in the grown material is highly desired.

What are the paths to find better material?

- **Further improvement of CZT growth : Already being improved for more than three decades. Did it reach a plateau?**

- **Improve CZT by adding some lattice hardening component : *We took this path by adding selenium.***

In our study, Se concentrations were varied from 1.5 % (atomic) to 7% (atomic), keeping the 10% Zn concentration for all the investigated compositions.
The lattice constant can be tuned by varying the Se concentrations.

Selenium has long been known as lattice hardening component in CdTe/CdZnTe matrix studied by the substrate community for IR/night vision applications.

Crystal growth

- CZTS ingots were grown by THM as well as vertical Bridgman Method (BM).
  - 6N purity CdZnTe and CdSe were used for synthesis of CZTS compound.
  - 6N purity Te was used as solvent for THM growth.
- Although BM technique is being used for crystal growth, our main thrust is THM growth of CZTS for its following advantages:
  - Low-temperature growth
  - Less chance of incorporation of impurities from the crucible during growth
  - Less/no chance of ampoule explosion
  - Enhanced purity of the ingot
  - Fewer defects due to the lower growth temperature

Optimizing THM-growth parameters

THM growth is highly sensitive to growth parameters.

i. Width of Te-rich solution zone
ii. Growth temperature
iii. Temperature gradient near the growth interface

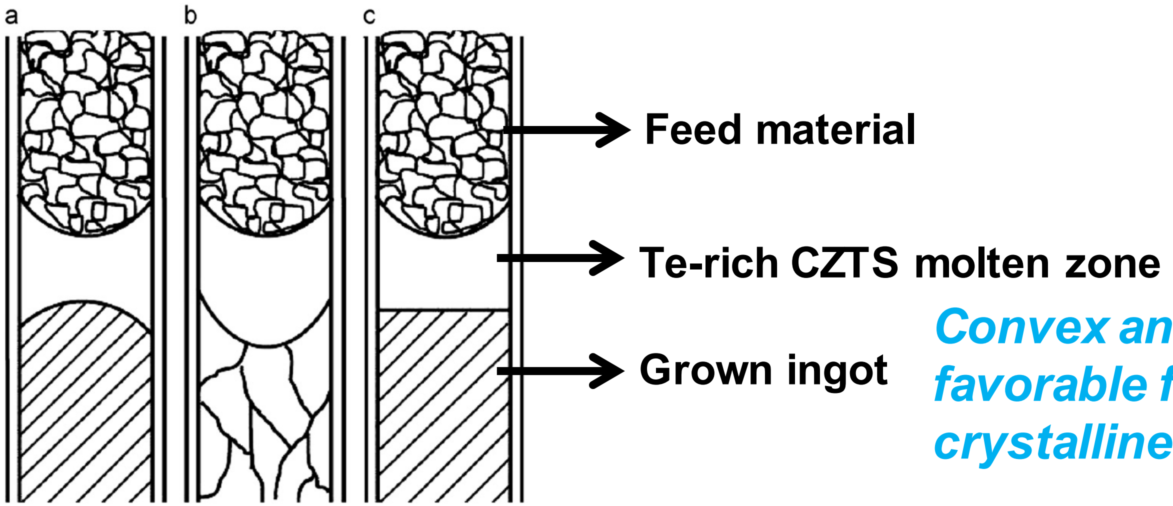

Schematic of growth interface shape
A) convex, B) concave and C) flat.

Convex and flat growth interfaces are favorable for growth of large grain and single crystalline ingots.

.

CZTS ingots

$Cd_{0.9}Zn_{0.1}Te_{0.93}Se_{0.07}$ ingots:

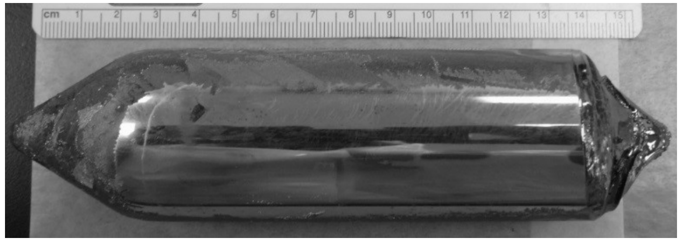

40-mm diameter ingot grown by BM (undoped).

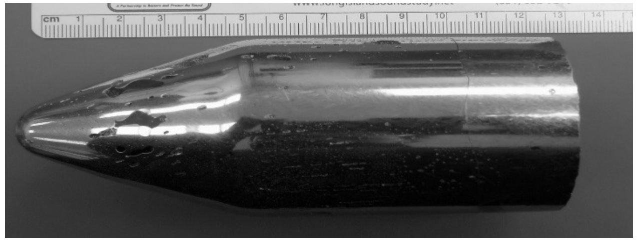

In-doped 52-mm diameter ingot grown by THM (fast cooled ingot).

$Cd_{0.9}Zn_{0.1}Te_{0.96}Se_{0.04}$ ingots:

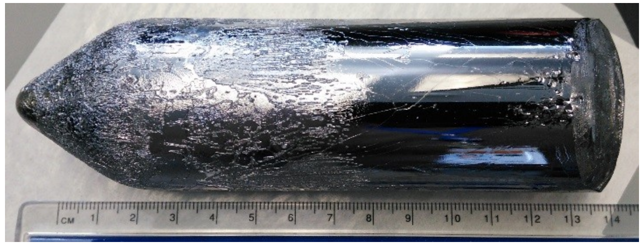

40-mm diameter ingot grown by BM (undoped).

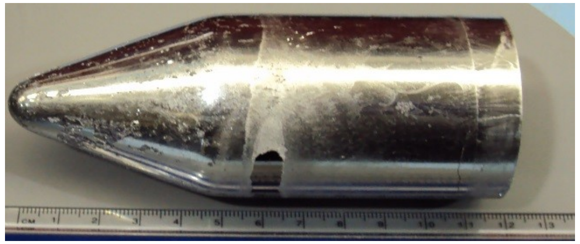

In-doped 52-mm diameter ingot grown by THM.

$Cd_{0.9}Zn_{0.1}Te_{0.98}Se_{0.02}$ ingots:

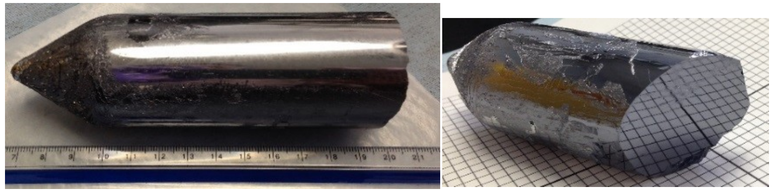

40-mm diameter ingot grown by BM (undoped).

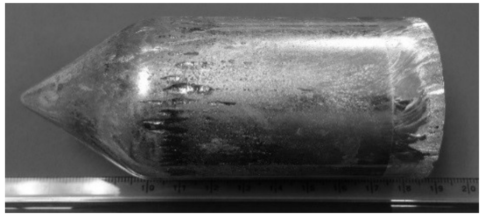

In-doped 52-mm diameter ingot grown by THM.

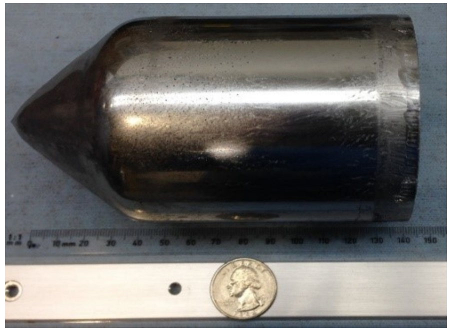

In-doped ~76-mm diameter ingot grown by THM.

Axial compositional distributions in CZTS

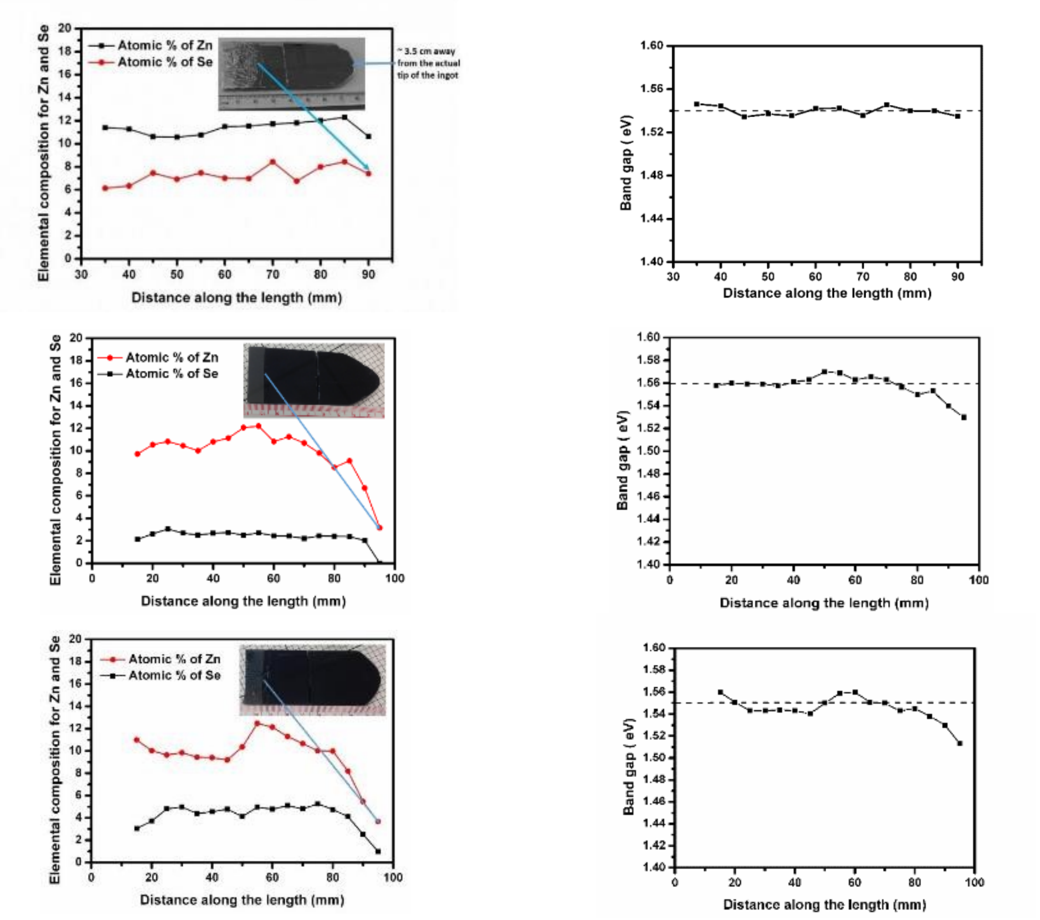

Zn and Se composition and calculated band-gap along the length of the THM-grown $Cd_{0.9}Zn_{0.1}Te_{0.93}Se_{0.07}$, $Cd_{0.9}Zn_{0.1}Te_{0.98}Se_{0.02}$ and $Cd_{0.9}Zn_{0.1}Te_{0.96}Se_{0.04}$ ingots: from top to bottom.

Composition of Zn and Se is uniform throughout the ingot for $Cd_{0.9}Zn_{0.1}Te_{0.93}Se_{0.07}$, especially the calculated band gap.

~90% of the THM-grown ingot shows uniform band gap for both 2 and 4% Se composition).

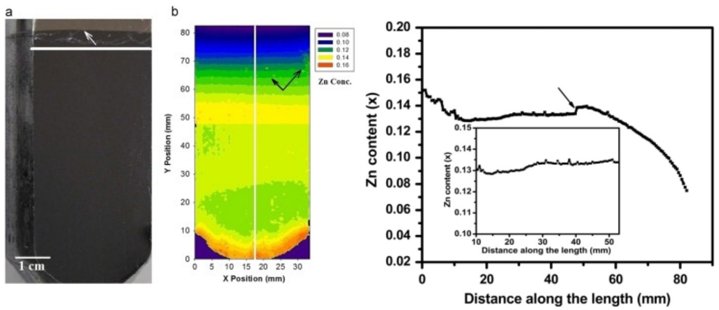

(a) THM-grown CZT ingot cut along the length, (b) Zn concentration mapping and (c) Zn concentration along the length of the ingot. Roy et al., J. Crystal Growth 347 (2012) 53.

Band gap along the length of Bridgman grown $Cd_{0.9}Zn_{0.1}Te_{0.96}Se_{0.04}$ ingot. Measured by elipsometry.

PL maps of THM-grown CZTS for 2-inch wafer (radial compositional distributions in CZTS)

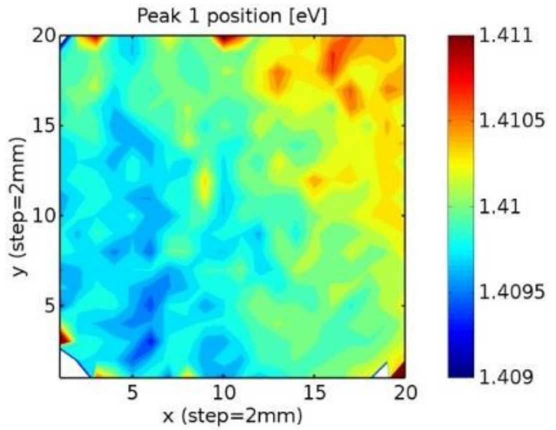

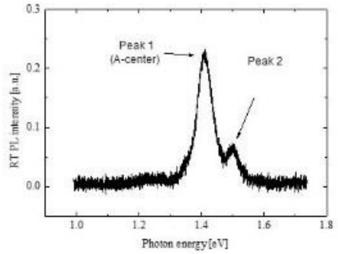

Room-temperature photoluminescence (PL) map of $Cd_{0.9}Zn_{0.1}Te_{0.93}Se_{0.07}$ two-inch wafer grown by THM. The map area is 4 x 4 cm^2. Step size is 2 mm.

Variation of the peak energy (peak 1) over the entire scan area, ΔE *is ~ 2 meV*, thus the composition and band-gap are highly uniform over the 4x4 cm^2 area.

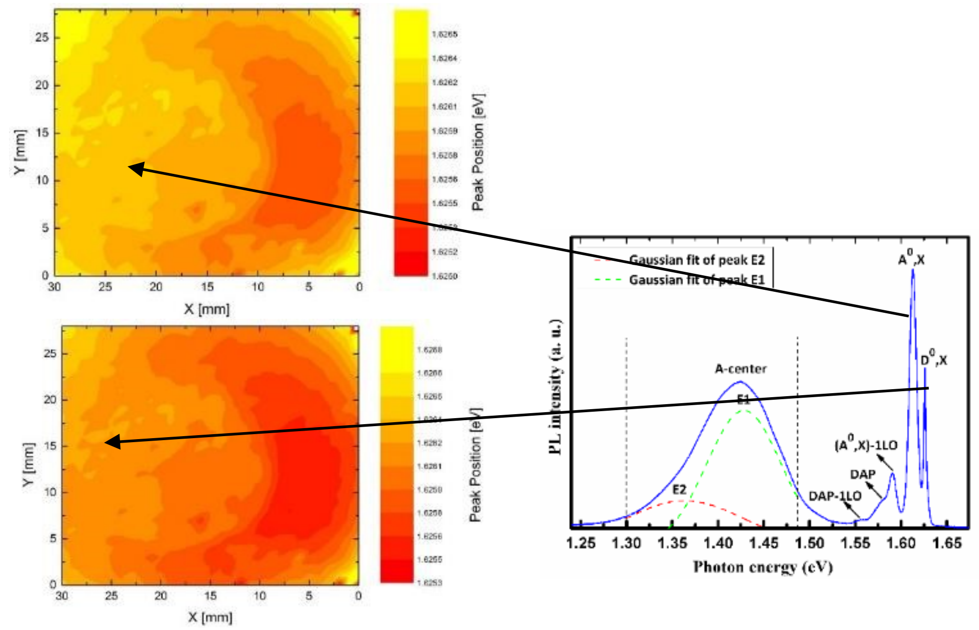

Low temperature (7 K) photoluminescence (PL) map of $Cd_{0.9}Zn_{0.1}Te_{0.98}Se_{0.02}$ two-inch wafer grown by THM. The map area is ~2.8x3 cm^2. Step size is 1 mm.

Variation of the peak energy (A^0,X and D^0,X) over the entire scan area , ΔE *is ~ 1.5 meV*, thus the composition and band-gap are highly uniform over the 2.8x3 cm^2 area.

Composition and band-gaps are highly uniform for both 2% and 7% Se CZTS wafers.

Sub-grain boundary and its network (X-ray topographic analyses of CZTS

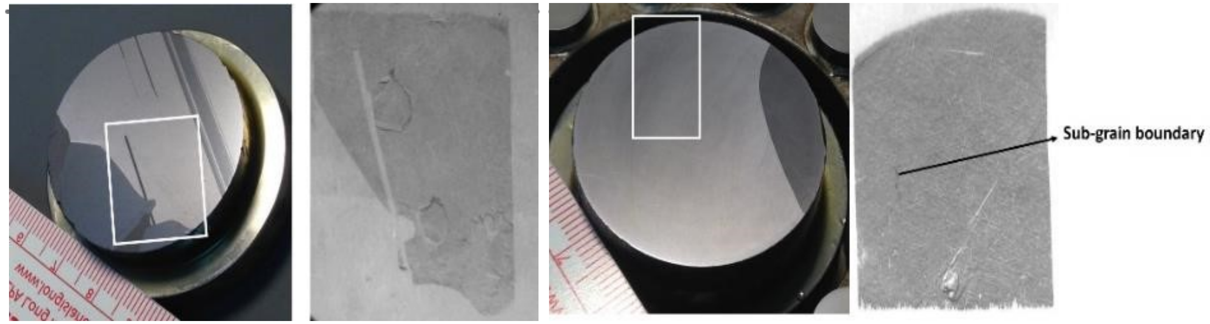

Picture of the lapped wafer (4-cm diameter) and the corresponding x-ray topographic image of the portion indicated (not to the scale) by the white rectangle of Bridgman grown $Cd_{0.9}Zn_{0.1}Te_{0.93}Se_{0.07}$ ingot

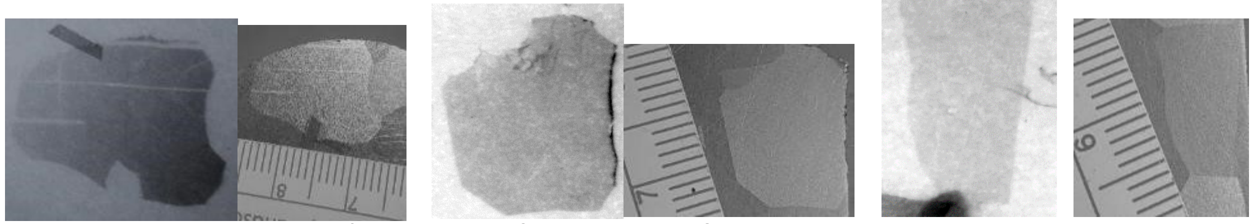

X-ray topographic pictures of THM-grown $Cd_{0.9}Zn_{0.1}Te_{0.93}Se_{0.07}$ *sample and the corresponding optical photography of the grains.*

Sub-grain boundary problem is alleviated in CZTS material.

The material is free from sub-grain boundary network, with occasional appearance of isolated sub-grain boundaries.

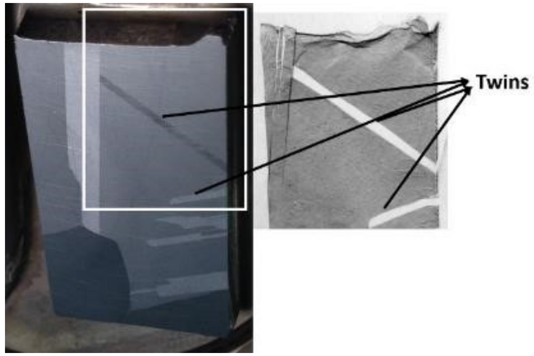

Picture of the lapped wafer (2.5-cm diameter) and the corresponding x-ray topographic image of the portion indicated (not to the scale) by the white rectangle of Bridgman grown $Cd_{0.9}Zn_{0.1}Te_{0.96}Se_{0.04}$ *ingot*

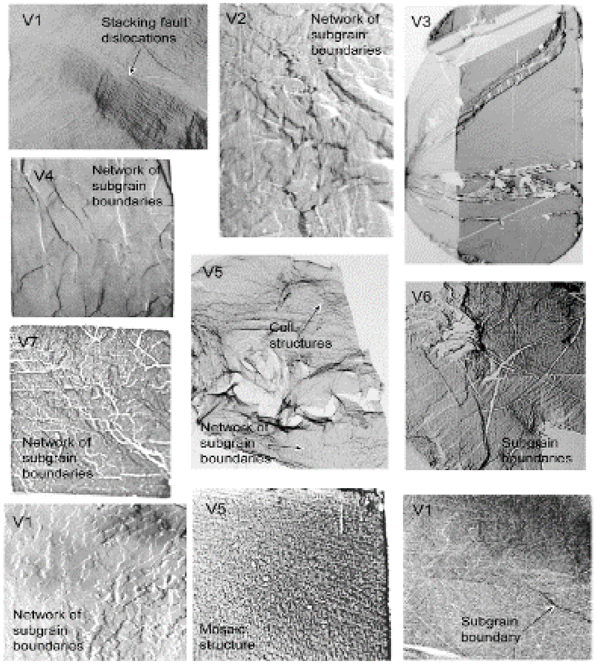

X-Ray diffraction topography images showing ~1 cm^2 areas of detector-grade CZT samples supplied by seven different vendors.

A. E. Bolotnikov et al., J. Cryst. Growth 379 (2013) 46.

Photograph of the sample, dimensions of the area exposed: 21x9 mm^2

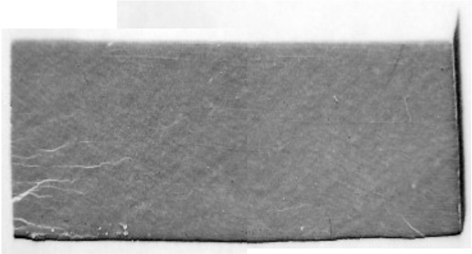

X-ray topographic picture of the THM-grown $Cd_{0.9}Zn_{0.1}Te_{0.96}Se_{0.04}$ *sample*

Presence of secondary phases in THM-grown *CZTS (IR Transmission Microscopy)*

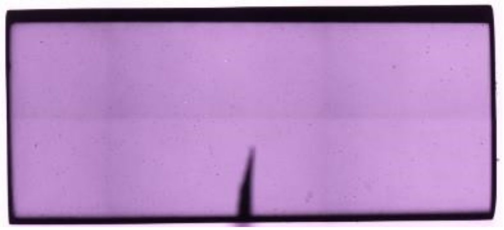

IR transmission picture of the THM grown $Cd_{0.9}Zn_{0.1}Te_{0.96}Se_{0.04}$ sample, sample dimensions: 4.6x4.5x10.7 mm^3

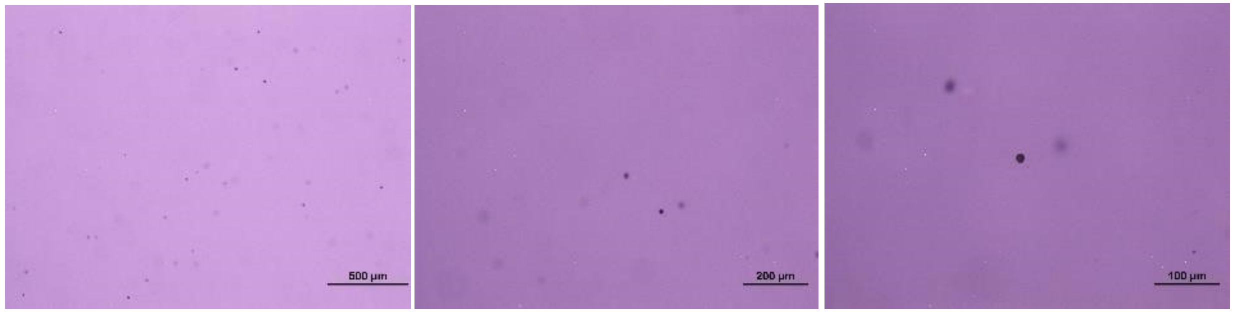

High magnification IR transmission microscopic images

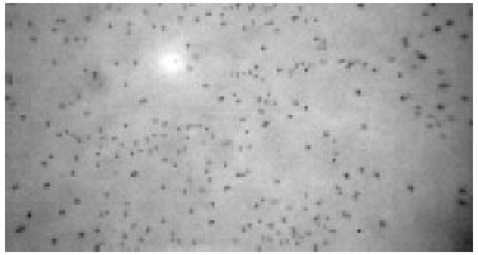

Typical Te inclusions in CdZnTe as observed through IR transmission microscopy.
S. Szeles, Phys. Stat. Sol. 241 (2004) 783.

IR transmission picture of the THM-grown $Cd_{0.9}Zn_{0.1}Te_{0.98}Se_{0.02}$ sample, sample dimensions: 8.2x7x1.55 mm^3

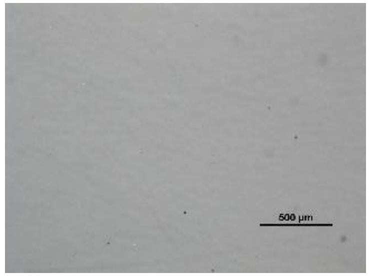

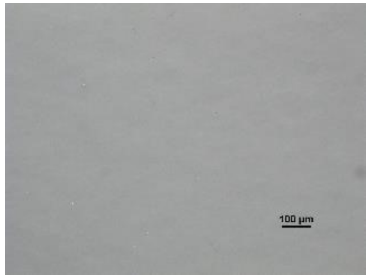

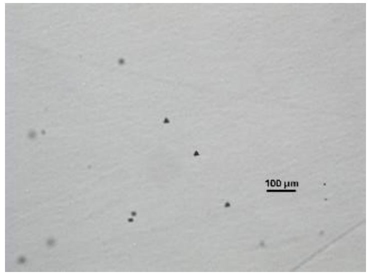

High magnification IR transmission microscopic images showing Te inclusions.

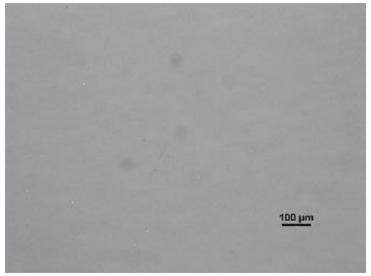

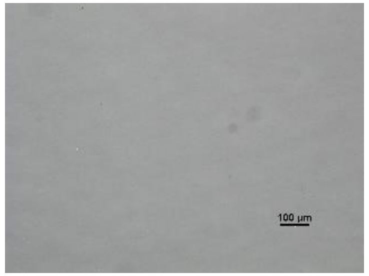

High magnification IR transmission microscopic image at three different positions.

Presence of secondary phases in THM-grown *CZTS (IR transmission microscopy)*

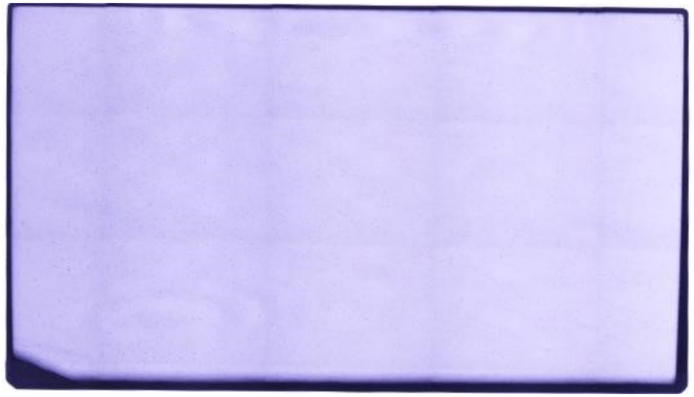

IR transmission picture of a THM-grown $Cd_{0.9}Zn_{0.1}Te_{0.85}Se_{0.015}$ sample. Sample dimensions: 11x10.8x19.4 mm^3

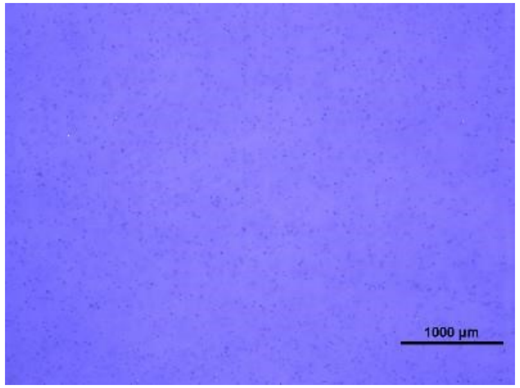

High magnification IR transmission microscopic images

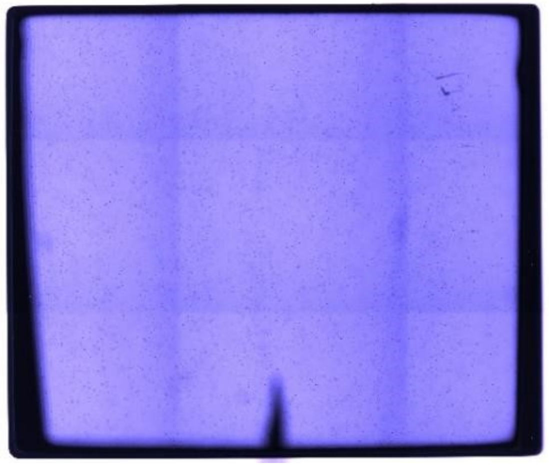

IR transmission picture of a THM-grown $Cd_{0.9}Zn_{0.1}Te_{0.85}Se_{0.015}$ sample. Sample dimensions: 8.1x9.4x11.1 mm^3

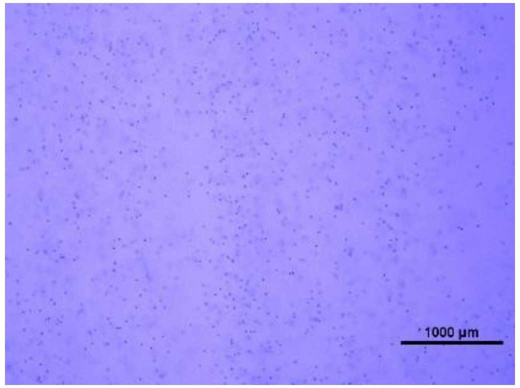

High magnification IR transmission microscopic images

Se with concentration 2% and above seems effective in reducing the concentration of Te inclusions/precipitations.

Present competitiveness of CZTS

CZT

- Non-unity segregation of Zn (*decreases overall yield*)
- Crystal defect (sub-grain boundary) network
- High concentrations of Te inclusions/precipitates

(*affect the yield of high-quality detectors*)

CZTS

- 90% of the ingot shows composition homogeneity *(increases the overall yield and has substantial potential to lower the cost)*
- Crystal defect (sub-grain boundary) network: Almost absent
- Low concentrations of Te inclusions/precipitates: Considerably less than CZT (with Se ≥ 2%)

Fewer defects can increase the yields and hence lower the cost of high-quality X- and gamma-ray detectors.

Se helps

- Modify Zn segregation coefficient
  - *Uniform material*
  - *High yield*
- Effective solution hardening to arrest sub-grain boundaries and their networks.
  - *Less defects, free from sub-grain boundary network*
  - *High yield*
- Reduce Te inclusion/precipitate concentration with increased Se content.
  - *Less defects*
  - *High yield*
- Reduce charge trapping centers.
  - *Better detector performance*
- Reduced thermal stress.
  - *Better detector performance*

Detector (FG geometry) response for THM-grown $Cd_{0.9}Zn_{0.1}Te_{0.98}Se_{0.02}$

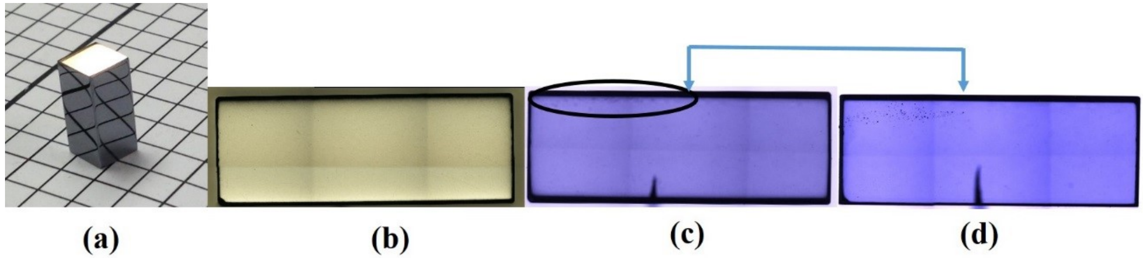

a) Optical photograph of the virtual Frisch grid detector sample with gold contacts, b) Optical scanning microscopic image of the detector in reflection mode, c) in IR transmission mode and d) IR transmission image observed through the upper surface of Fig. c). The detector dimensions: 5x5x12.3 mm^3.

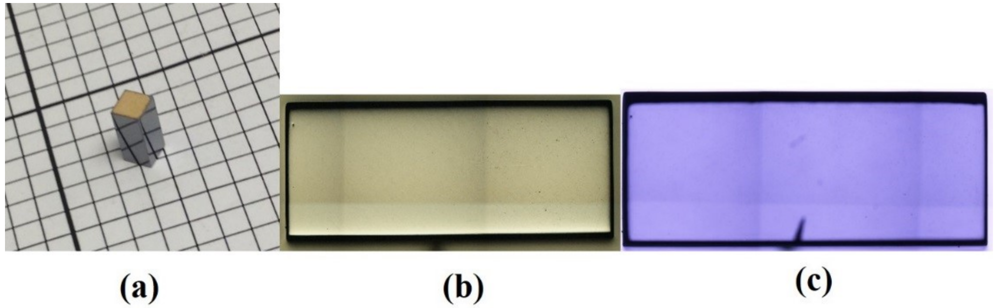

a) Optical photograph of the virtual Frisch grid detector sample with gold contacts, b) Optical scanning microscopic image of the detector in reflection mode and c) in IR transmission mode. The detector dimensions: 4.5x4.5x10.8 mm^3.

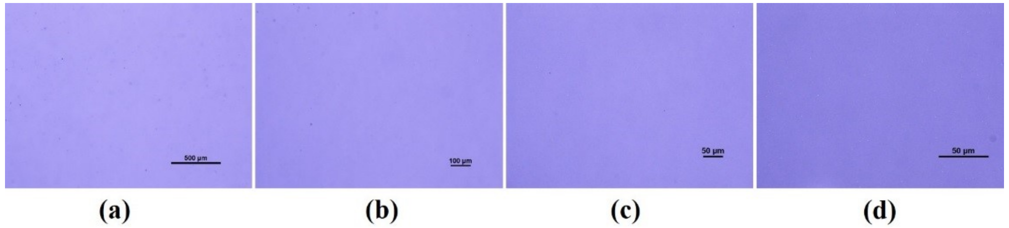

High-magnification IR transmission microscopic images with increased magnification from left to right.

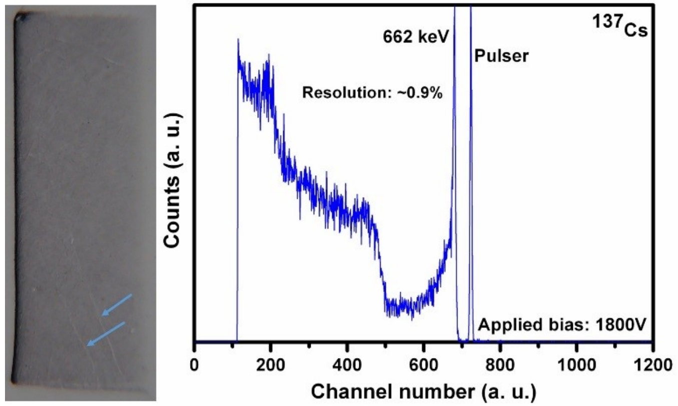

X-ray topographic image of the whole detector (left) and the pulse height spectrum of the virtual Frisch grid detector for a ^{137}Cs source at room temperature.

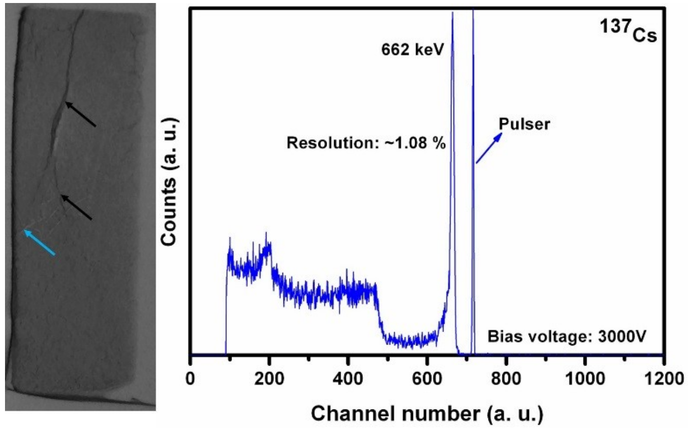

X-ray topographic image of the whole detector (left) and the pulse height spectrum of the virtual Frisch grid detector at room temperature for a ^{137}Cs source.

Detector (FG geometry) response for THM-grown $Cd_{0.9}Zn_{0.1}Te_{0.98}Se_{0.02}$

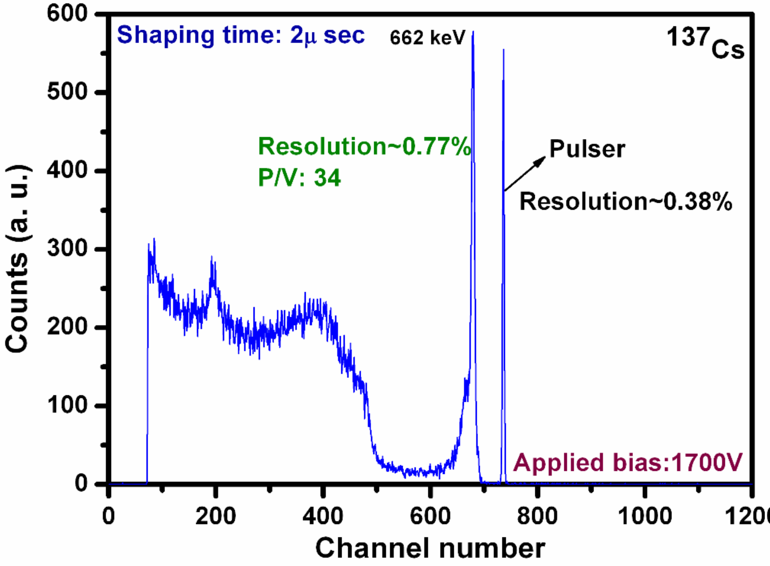

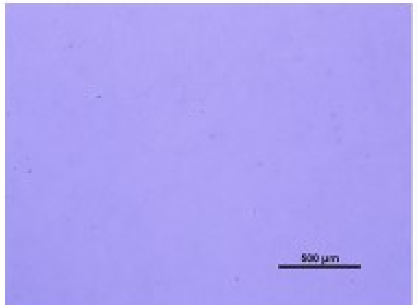

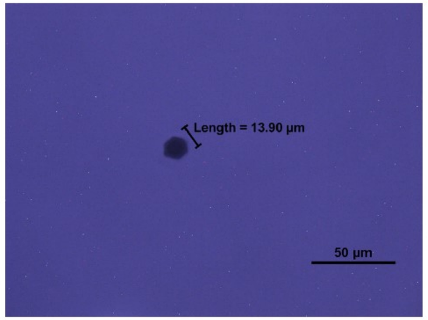

Pulse height spectrum of ^{137}Cs source of Frisch-grid detector fabricated from as-grown $Cd_{0.9}Zn_{0.1}Te_{0.98}Se_{0.02}$ THM ingot.

Detector dimensions: 3.5x3.5x9.15mm^3.

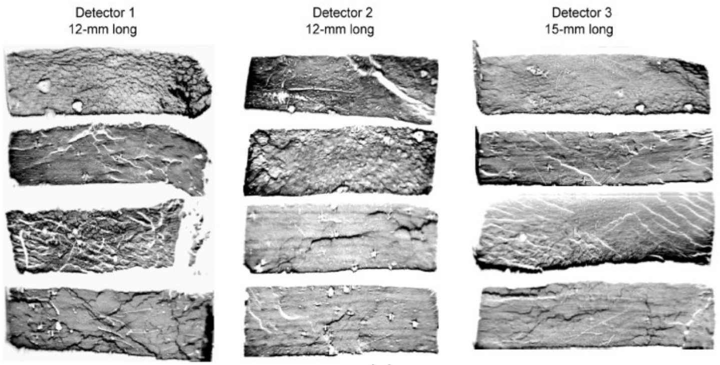

X-ray topography of CZT detectors

A.E. Bolotnikov et al. SPIE Proc. Vol 8142 (2011) 814206

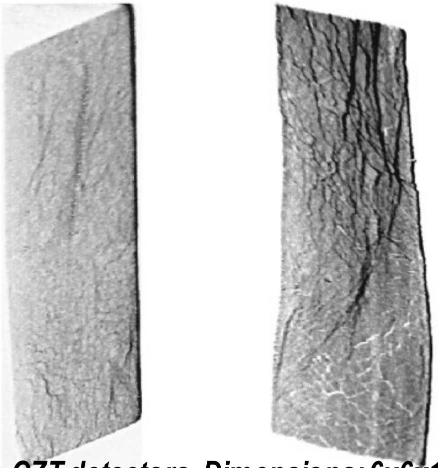

X-ray topography of two CZT detectors, Dimensions: 6x6x15 mm^3

A.E. Bolotnikov et al. J. Cryst. Growth 379 (2013) 46

Detector (FG geometry) response for THM-grown $Cd_{0.9}Zn_{0.1}Te_{0.98}Se_{0.02}$

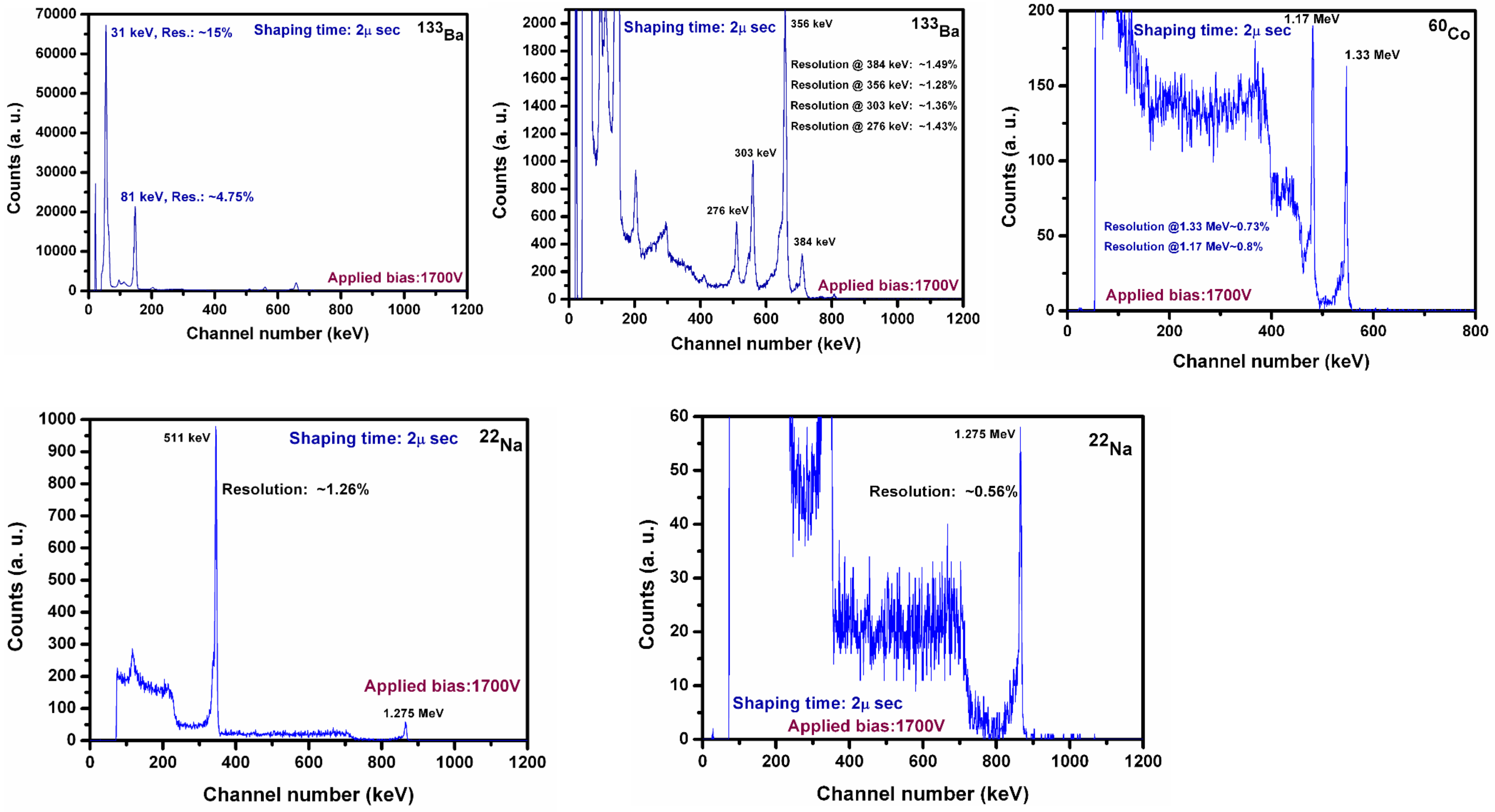

Pulse height spectra of ^{133}Ba, ^{60}Co and ^{22}Na for a Frisch-grid detector fabricated from a THM-grown $Cd_{0.9}Zn_{0.1}Te_{0.98}Se_{0.02}$ ingot.

All the spectra are from as-grown material and as-measured with no corrections for charge loss.

Comparison of CZT and CZTS

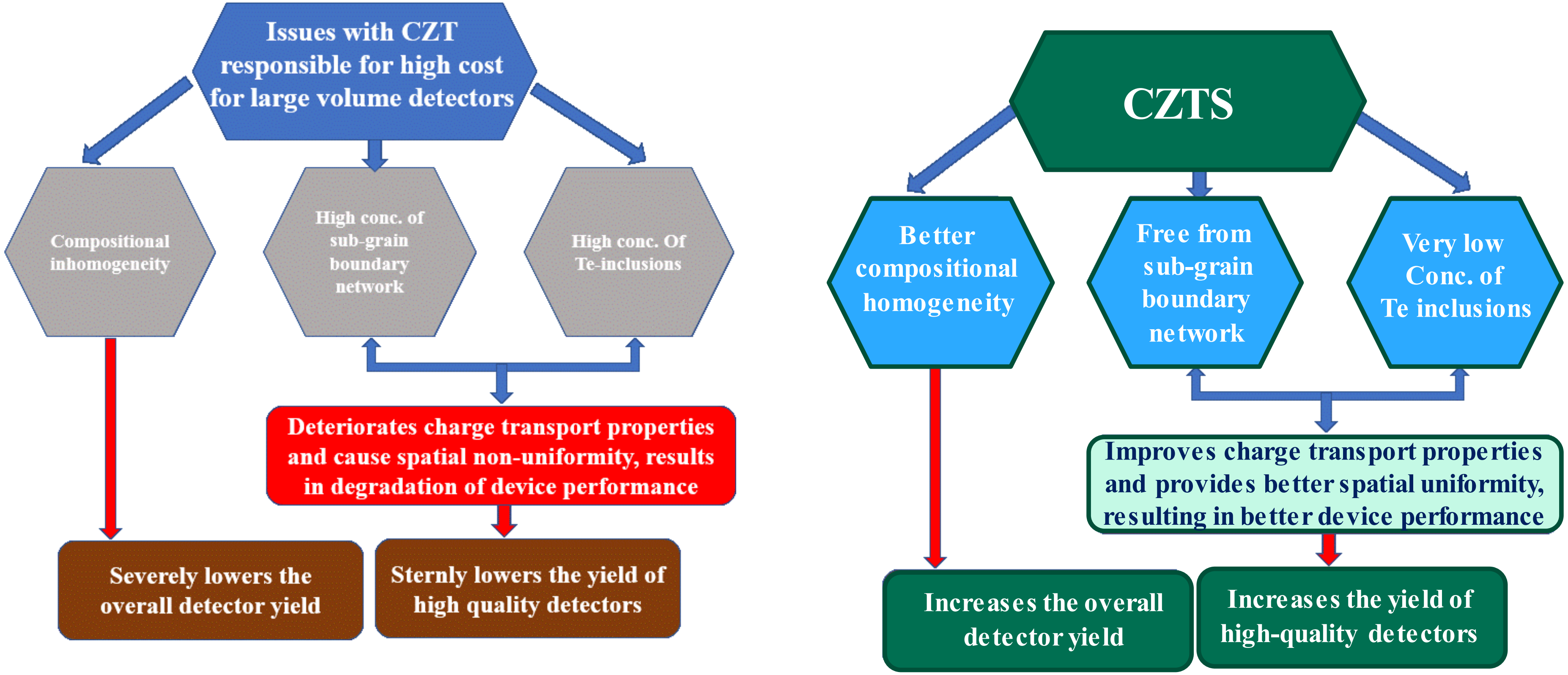

Future of CZTS is bright. The material is capable of replacing CZT at a much lower cost.

The new quaternary CZTS is being widely accepted by industry and academia. General Electric recently reported the superior properties of CZTS as compared to CZT for medical imaging applications.

Can we further improve the detector performance of CZTS?

6N purity CZT (raw material)

CZT 1

Element	Concentration [ppb at]
Cr	<3
Fe	34
Ni	<5
Cu	<15
Sn	<45
Pb	<2

CZT 2

Element	Concentration [ppb at]
Cr	<3
Fe	110
Ni	<4
Cu	<8
Sn	<30
Pb	<2

6N purity $Cd_{0.9}Zn_{0.1}Te_{0.98}Se_{0.02}$ grown by THM

Ingot #1

Element	Concentration [ppb at]
Cr	<20
Fe	42
Ni	<4
Cu	22
Sn	<100
Pb	10

Ingot #2

Element	Concentration [ppb at]
Cr	36
Fe	42
Ni	16
Cu	<4
Sn	<100
Pb	11

The impurities present in THM-grown $Cd_{0.9}Zn_{0.1}Te_{0.98}Se_{0.02}$ are 3-8 times higher compared to CZT raw material.

While for commercial THM grown CZT contain (ppb at):
Cr-ND, Fe-22, Ni-ND, Cu-ND

ND- Not Detected

J.J. McCoy et al., J. Electronic Materials 48, 4226 (2019).

We expect to improve the energy resolution (as measured) at 662 keV to be between 0.4-0.5 % for THM-grown $Cd_{0.9}Zn_{0.1}Te_{0.98}Se_{0.02}$ by using purified starting material.

CZTS has the potential to approach Ge-like performance, while working at room temperature.

CdZnTeSe perhaps qualifies to be at the top of the pyramid of semiconductor detector family

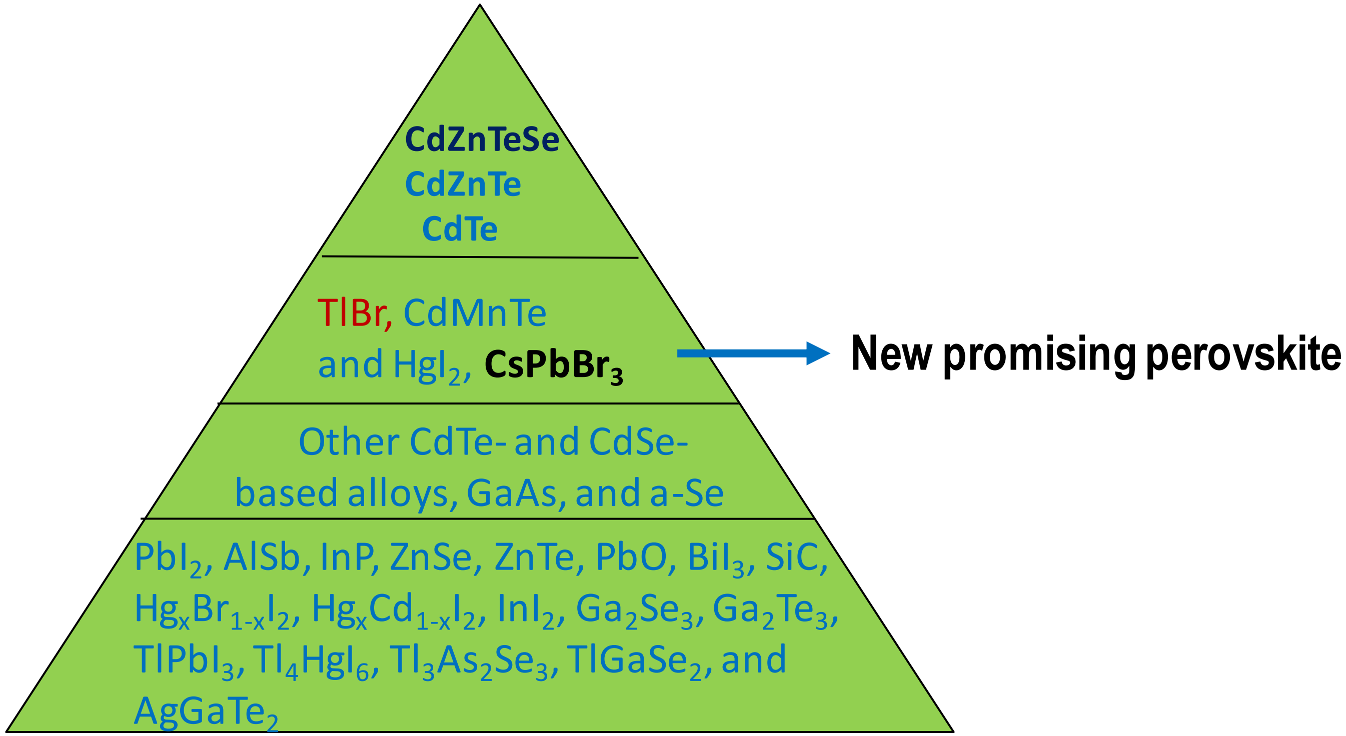

First, some issues suffered by CdZnTeSe need to be resolved:

- High concentrations of performance limiting impurities

Acknowledgement

This work was partially supported by U.S. Department of Energy/NNSA, Office of Defense Nuclear Nonproliferation Research and Development and MSIPP. The author (U. Roy) acknowledges partial support of LDRD funding from SRNL.

Thank you for your kind attention !